Ricerche di Matematica
https://doi.org/10.1007/s11587-022-00728-y

Unsteady MHD fluid flow over an inclined plate, inclined magnetic field and variable temperature with Hall and Ion-slip current

Md. Rafiqul Islam[1] · **Sonia Nasrin**[2] · **Md. Mahmud Alam**[3]

Received: 16 February 2022 / Revised: 4 July 2022 / Accepted: 16 August 2022

Abstract
This research looks at the Hall and Ion-slip currents with time variation in an unstable, incompressible, viscous fluid electrically conducting free convection flow that passes over an electrically non-conducting inclined plate in the presence of an inclined magnetic field. The fluid flow is generated by the moving and oscillating plate, and it is also influenced by the magnetic force, gravitational force, and viscous force. The buoyancy forces are produced by temperature and concentration variance in the gravity field due to the oscillating plate in its own plane. The governing equations are derived from the Navier–Stokes equation, energy equation, and concentration equation and then applied to the boundary layer approximation. The magnetic Reynolds number of flows is kept relatively small, so this analysis has not used the magnetic induction equation. On the velocity distribution, the angle of inclination has a retarding impact. The results of this study have been shown to explain the drag on flow at inclined surfaces instantly. The impact of the relevant parameters on fluid velocity, temperature, and concentration distributions has been explained and visualized using graphs. Numerical data for skin friction, rate of heat transmission, and mass transfer in terms of shear stress, Nusselt, and Sherwood numbers are visualized graphically.

Keywords MHD fluid · Heat transfer · Mass transfer · Inclined angle · Hall and Ion-slip current

Mathematics Subject Classification 76W05

✉ Md. Rafiqul Islam
mribsmrstu@yahoo.com

[1] Department of Mathematics, Bangabandhu Sheikh Mujibur Rahman Science and Technology University, Gopalganj 8100, Bangladesh

[2] Department of Mathematics, Jagannath University, Dhaka 1100, Bangladesh

[3] Mathematics Discipline, Khulna University, Khulna 9208, Bangladesh

Published online: 09 September 2022

List of symbols

$\mathbf{q}$	Fluid velocity vector
$\mathbf{J}$	Current density vector
u	Velocity components along x-axis
v	Velocity components along y- axis
w	Velocity components along z- axis
β	Volumetric coefficient of thermal expansion
β^*	Volumetric coefficient of mass expansion
B_0	Constant magnetic induction along y-directions
ω	Acceleration frequency
ω_e	Cyclotron frequency
ρ	Density of the fluid
σ	Conductivity of the fluid
τ_e	Electron collision time
c_p	Specific heat at the constant pressure
k_T	Thermal diffusion ratio
υ	Kinematic viscosity
$\mathbf{B}$	Magnetic field vector
$\mathbf{g}$	Gravitational acceleration
U_0	Constant uniform velocity
α	Inclined angle
t	Time
Δt	Time increment
τ	Maximum time
c_s	Concentration susceptibility
σ'	Electric conductivity
μ	Fluid viscosity coefficient
μ_e	Magnetic permeability
β_e	Hall parameter
β_i	Ion-slip parameter
u^*	Dimensionless velocity component in x-axis
v^*	Dimensionless velocity component in y-axis
t^*	Dimensionless time
ω^*	Dimensionless acceleration parameter
θ	Dimensionless temperature
φ	Dimensionless fluid concentration
D_m	Mass diffusion coefficient
T	Temperature of the fluid
T_w	Constant temperature near the plate
T_∞	Outside boundary layer temperature
C	Concentration in the fluid
C_w	Constant concentration near the plate
C_∞	Outside boundary layer concentration
H_a	Hartmann number
G_r	Thermal Grashof number

G_m	Solutal Grashof number
P_r	Prandtl number
S_c	Schmidt number
D_f	Dufour number
τ_{xL}	Local primary shear stress
τ_{zL}	Local secondary shear stress
Nu_L	Local Nusselt number
Sh_L	Local Sherwood number
τ_{xA}	Average primary shear stress
τ_{zA}	Average primary shear stress
Nu_A	Average Nusselt number
Sh_A	Average Sherwood number

1 Introduction

The impact of the magnetic field on magneto-hydrodynamic (MHD) fluid flow is crucial for experimental and theoretical applications in magnetic material processing, astronomy, nuclear engineering, geophysics, and industry. Hall and Ion-slip currents influence the electrically conducting fluid in a magnetic field. Therefore, in chemical and mechanical engineering, the mechanism of electrically conducting flow in a magnetic field with Hall and Ion-slip current is also important. The effect of the inclined magnetic field on the vertical line is also investigated to understand the physical condition of the problem. A pile of research works have been done regarding the fluid flow with magnetic field, Hall and Ion-slip Current. The following paragraph provides references for part of our study.

Abel and Veena [1] discussed the flow of viscoelastic fluids through a saturated porous medium with internal heat production and frictional heat on the stretching surface. Abernathy [2] studied a free-streamline theory for a flat plate leaning towards an infinite flow field at an angle of attack. Measurement of the free-rotation layers, the frequency of the rotation path, and the pressure behind a sharp-edged plate are effective in plate attack angle and lateral contraction of the flow. Ajay [3] investigated the combined effects of Hall current, viscous dissipation, joule heating, and thermal expansion on the magneto-hydrodynamic free circulation flow of electrically conductive fluid, including mass transfer on infinitely vertical porous plates. Angirasa and Peterson [4] discussed a numerical study on the natural transfer of heat from an isothermal vertical surface to a stable layer with a fluid-saturated thermal layer perforated. Basant and Malgwi [5] have analyzed the effect of Hall and Ion-slip current on the free circulation of an incompressible viscous fluid flow in a vertical microchannel with an induced magnetic field. Beg et al. [6] performed a numerical solution for magnetohydrodynamic incompressible, viscous fluid flow in a rotating perforated channel comprising two infinite parallel plates with Hall current and an inclined magnetic field. Bhpendra et al. [7] presented the Hall current effect on the unsteady viscous incompressible mixed convective fluid flow past a vertical infinite porous plate with the heat source (or sink). Daniel and Daniel [8] analyzed two insoluble convective currents and heat

transfer with a porous plate across a gradient channel with a pressure gradient. Eraslan [9] has revealed a wholly improved temperature distribution for MHD channels with the Hall effect. They have found perforated structures material constants and can control fluid flow with different fluid efficiency. Gupta [10] studied the heat and mass transfer of electromagnetic fluid flow in a stretched sheet by suction and blowing. Javeri [11] studied the effect of the combined Hall current, Ion-slip, Joule heating, and viscous dissipation on the MHD heat transfer flow in a channel. The effects of thermal radiation, heat, and mass transfer on MHD heat and mass transfer free circulation flow through an accelerated curved plate embedded in a saturated porous medium have been investigated by Jyotsna et al. [12]. Kumar and Singh [13] investigated the natural circulation of heat transfer through a porous medium perpendicular to the isothermal surface under the influence of thermal stratification. Navnet et al. [14] examined the effect of inclined magnetic fields on unsteady viscous, non-compressible fluid flows on a vertical moving plate with variable temperature. Opanuga et al. [15] analyzed the rate of entropy formation on a few stress fluids in the presence of Hall and Ion-slip currents, including velocity slip and temperature jump. The effect of the flow is the generalized Couette flow of a viscous conducting fluid under an inclined magnetic field is analyzed by Prasada et al. [16]. Rajput and Gupta [17] considered unsteady free-convection MHD fluid flow along with an exponentially accelerated plate through a perforated medium with a variable temperature, an inclined magnetic field, and steady mass diffusion. Ram [18] investigated the effects of Hall and ion-slip currents on a rare gas that generates heat through free convection in a rotating frame with a strong magnetic field normal to the plate. Rishab et al. [19] investigated the viscoelastic flow of an electrically conducting fluid through two parallel plates filled with a perforated medium placed in an inclined magnetic field with heat and mass transfer. Sato [20] analyzed the electrical conductivity of ionized gas with the Hall effect, where the conductivity is represented by a tensor in the same shape for both partially and fully ionized gas. Seth et al. [21–23] investigated the Hall effects in the Viscous, ionized Gas Flow between two parallel plates under a transverse magnetic field; Electro-Magnetic Couette flows in the presence of an inclined magnetic field with rotation; The Hall current effect and rotational effect on the Hartmann's flow of an incompressible viscous electrically conducting fluid in the presence of the inclined magnetic field are discussed. And they also studied the MHD free-convection flow of an incompressible, viscous, electrically conducting fluid through a saturated porous medium in the presence of inclined magnetic fields. Suman and Nazibuddin [24] analyzed the unsteady MHD fluid flow with mass transfer through an infinitely inclined plate. The velocity is strengthened between a poachy porous medium with an alternating temperature. Singh et al. [25] explored how unsteady hydromagnetic heat and mass transfer with current and rotation natural convection flows through an accelerating vertical plate in the presence of heat and mass diffusions. In another experiment, Singh et al. [26] also observed an unstable MHD natural convection flow of a rotating walters'-b fluid across an oscillating plate with variable temperature and concentration. Singh et al. ([27]-[28]) studied the effects of Hall and Ion-slip currents on the MHD free convective flow of a viscoelastic fluid through a porous regime in an inclined channel with a moving magnetic field, as well as the mixed convection flow of a viscoelastic fluid through a vertical porous channel with rotation, heat radiation,

and chemical reaction. Krishna et al. [29] examined the impacts of Hall and Ion-slip currents on unsteady magneto-hydrodynamic free convective flow with rotation analytically through an exponentially accelerating inclined plate immersed in a saturated porous media, taking into account the effects of inclined angle. This study has been investigated the result of numerical solution of the unsteady magneto-hydrodynamic fluid flow over an inclined plate with an inclined induced magnetic field, time variation measurements by the effect of Dufour, Hall, and Ion-slip currents.

2 Governing equations and mathematical model

The basic governing equations are in vector form:

Continuity equation:

$$\nabla \,.\, \mathbf{q} = 0 \tag{1}$$

Momentum equation:

$$\frac{\partial \mathbf{q}}{\partial t} + (\mathbf{q} \,.\, \nabla)\, \mathbf{q} = \mathbf{F} - \frac{1}{\rho}\nabla p + \upsilon \nabla^2 \mathbf{q} \tag{2}$$

Energy equation:

$$\frac{\partial T}{\partial t} + (\mathbf{q} \,.\, \nabla) T = \frac{k}{\rho C_p}\Delta^2 T + \frac{D_m k_T}{c_s c_p}\Delta^2 C \tag{3}$$

Concentration equation:

$$\frac{\partial C}{\partial t} + (\mathbf{q} \,.\, \nabla) C = D_m \Delta^2 C \tag{4}$$

Let an electrically non-conducting plate be fixed at $y = 0$ along the x-axis in the fluid, which makes an angle α with a vertical line, and y-axis is normal to the $xz-$ plane. Consider an unsteady magneto-hydrodynamic incompressible viscous electrically conducting free convective flow is taken along the x-axis. Let u, v and w are the velocity components along directions x-, y-, and z-axis respectively. Initially, the plate and fluid are considered to be at rest, it is assumed that fluid velocity, temperature, and fluid concentration are fixed at $u = 0, \quad w = 0, \quad T = T_\infty$ and $C = C_\infty$ respectively. At the time $t > 0$, the plate oscillates and moves in its plane with a velocity $U_0 \cos \omega t$ along x-axis. The temperature of the plate and the concentration are raised from $T_\infty + (T_w - T_\infty)\frac{U_0^2 t}{\upsilon}$ to T_∞ and $C_\infty + (C_w - C_\infty)\frac{U_0^2 t}{\upsilon}$ to C_∞ with time t. The magnetic Reynolds number of flows is taken very small, so that induced magnetic field equation is not considered in our analysis.

Since the electromagnetic fluid flow is influenced by the Hall and Ion-slip current, therefore due to the application of Hall, and Ion-slip current, the generalized Ohm's

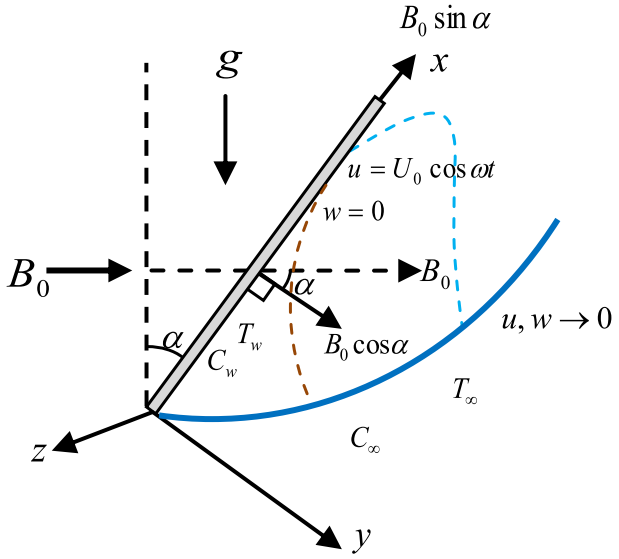

Fig. 1 Physical configuration and coordinate system

law may state as follows:

$$\mathbf{J} + \frac{\beta_e}{B_0}(\mathbf{J} \wedge \mathbf{B}) = \sigma(\mathbf{q} \wedge \mathbf{B}) + \frac{\omega_e \tau_e \beta_i}{B_0^2}(\mathbf{J} \wedge \mathbf{B}) \wedge \mathbf{B} \tag{5}$$

where $\omega_e \tau_e = \beta_e$ may treat as Hall parameter, $\mathbf{B}$ is the magnetic field vector. A uniform transverse magnetic field strength B_0 has been imposed horizontally, *i.e.* it acts at a right angle to the plate when the inclined angle of the plate $\alpha = 0$. When the coordinate system as well as the plate makes an angle α with the vertical line, then this magnetic field vector becomes $\mathbf{B} = (B_0 \sin\alpha \ , \ B_0 \cos\alpha \ , \ 0)$. Physical model of the system is shown in the following Fig. 1.

The x-component momentum equation reduces to the boundary layer equation if the only contribution to the body force is made by the gravity, the body force per unit volume is $F_x = -g\cos\alpha$, where g is the local acceleration due to the gravity. There is no body force in the y-direction and z-direction i.e. $F_y = 0$ and $F_z = 0$. The applied pressure p is a function of x only. The x-component pressure gradient $\frac{\partial p}{\partial x} = -\rho_\infty g \cos\alpha$, where ρ_∞ is the density of the surrounding fluid at the temperature T_∞. Therefore

$$F_x - \frac{1}{\rho}\frac{\partial p}{\partial x} = -g\cos\alpha + \frac{\rho_\infty g}{\rho}\cos\alpha = -g\cos\alpha\left(\frac{\rho - \rho_\infty}{\rho}\right)$$

For small difference, the density difference term, $\rho - \rho_\infty$ is related to the temperature difference $T - T_\infty$ and the mass difference $C - C_\infty$ through the volumetric coefficient of thermal expansion β and the volumetric coefficient of mass expansion β^* by the

relation

$$\left(\frac{\rho-\rho_\infty}{\rho}\right) = -\beta(T-T_\infty) - \beta^*(C-C_\infty)$$
$$\therefore \quad F_x - \frac{1}{\rho}\frac{\partial p}{\partial x} = g\beta\cos\alpha(T-T_\infty) + g\beta^*\cos\alpha(C-C_\infty) \tag{6}$$

It is assumed that the plate is of semi-infinite extended length, then all the physical variables in the problem are functions of x, y and t. Therefore the problem is two-dimensional. Based on the above-mentioned assumptions with boundary layer approximations and utilizing generalized Ohm's law with Hall current and Ion-slip current, the governing Eqs. (1) to (4) of fluid are as follows.

$$\frac{\partial u}{\partial x} + \frac{\partial v}{\partial y} = 0 \tag{7}$$

$$\frac{\partial u}{\partial t} + u\frac{\partial u}{\partial x} + v\frac{\partial u}{\partial y} = g\beta\cos\alpha\ (T-T_\infty) + g\beta^*\cos\alpha\ (C-C_\infty) + \upsilon\frac{\partial^2 u}{\partial y^2} - \frac{\sigma B_0^2}{\rho}(\Gamma_1 u + \Gamma_2 w) \tag{8}$$

$$\frac{\partial w}{\partial t} + u\frac{\partial w}{\partial x} + v\frac{\partial w}{\partial y} = \upsilon\frac{\partial^2 w}{\partial y^2} + \frac{\sigma B_0^2}{\rho}(\Gamma_2 u - \Gamma_3 w) \tag{9}$$

$$\frac{\partial T}{\partial t} + u\frac{\partial T}{\partial x} + v\frac{\partial T}{\partial y} = \frac{k}{\rho c_p}\frac{\partial^2 T}{\partial y^2} + \frac{D_m k_T}{c_s c_p}\frac{\partial^2 C}{\partial y^2} \tag{10}$$

$$\frac{\partial C}{\partial t} + u\frac{\partial C}{\partial x} + v\frac{\partial C}{\partial y} = D_m\frac{\partial^2 C}{\partial y^2} \tag{11}$$

with corresponding boundary conditions:

$$\begin{aligned} t \le 0 \ &: \quad u = 0,\ w = 0,\ T = T_\infty,\ C = C_\infty \\ t > 0 \ &: \begin{cases} u = U_0\cos\omega t\ ,\ w = 0,\ T = T_\infty + (T_w - T_\infty)\dfrac{U_0^2 t}{\upsilon},\ C = C_\infty + (C_w - C_\infty)\dfrac{U_0^2 t}{\upsilon} & \text{at } y = 0 \\ u = 0\ ,\ w = 0,\ T \to T_\infty,\ C \to C_\infty & \text{as } y \to \infty \end{cases} \end{aligned} \tag{12}$$

where, $\Gamma_1 = \frac{(1+\beta_e\beta_i\cos\alpha)\cos^2\alpha}{(1+\beta_e\beta_i)(1+\beta_e\beta_i\cos^2\alpha)+\beta_e^2\cos^2\alpha}$, $\Gamma_2 = \frac{\beta_e\cos^3\alpha}{(1+\beta_e\beta_i)(1+\beta_e\beta_i\cos^2\alpha)+\beta_e^2\cos^2\alpha}$ and $\Gamma_3 = \frac{(1+\beta_e\beta_i)\cos^2\alpha}{(1+\beta_e\beta_i)\,(1+\beta_e\beta_i\cos^2\alpha)+\beta_e^2\cos^2\alpha}$

2.1 Non-dimensional analysis

The following non-dimensional variables are introduced to make the dimensionless form of the above equations.

$$x^* = \frac{U_0}{\upsilon}x\,,\quad y^* = \frac{U_0}{\upsilon}y\,,\quad u^* = \frac{u}{U_0}\,,\ v^* = \frac{v}{U_0}\,,\ w^* = \frac{w}{U_0}\ ,\ \omega^* = \frac{v}{U_0^2}\omega,\ t^* = \frac{U_0^2}{\upsilon}t\,,\ \theta = \frac{T-T_\infty}{T_w-T_\infty}\,,\quad \varphi = \frac{C-C_\infty}{C_w-C_\infty}$$

Removing the asterisk sign, the non-dimensional form of the Continuity equation, Momentum equations, Energy equation and Concentration equation as follows:

$$\frac{\partial u}{\partial x} + \frac{\partial v}{\partial y} = 0 \tag{13}$$

$$\frac{\partial u}{\partial t} + u\frac{\partial u}{\partial x} + v\frac{\partial u}{\partial y} = G_r\theta\cos\alpha + G_m\varphi\cos\alpha + \frac{\partial^2 u}{\partial y^2} - H_a(\Gamma_1 u + \Gamma_2 w) \tag{14}$$

$$\frac{\partial w}{\partial t} + u\frac{\partial w}{\partial x} + v\frac{\partial w}{\partial y} = \frac{\partial^2 w}{\partial y^2} + H_a(\Gamma_2 u - \Gamma_3 w) \tag{15}$$

$$\frac{\partial \theta}{\partial t} + u\frac{\partial \theta}{\partial x} + v\frac{\partial \theta}{\partial y} = \frac{1}{P_r}\frac{\partial^2 \theta}{\partial y^2} + D_f\frac{\partial^2 \varphi}{\partial y^2} \tag{16}$$

$$\frac{\partial \varphi}{\partial t} + u\frac{\partial \varphi}{\partial x} + v\frac{\partial \varphi}{\partial y} = \frac{1}{S_c}\frac{\partial^2 \varphi}{\partial y^2} \tag{17}$$

With the corresponding boundary conditions:

$$\begin{aligned} t \le 0\ &:\quad u = 0,\ \ w = 0,\ \ \theta = 0,\ \ \varphi = 0 \\ t > 0\ &:\begin{cases} u = \cos\omega t\ ,\ w = 0,\ \ \theta = t\ ,\ \ \varphi = t\ \text{ at }\ y = 0 \\ u = 0\ \ ,\ \ w = 0,\ \ \theta \to 0,\ \ \varphi \to 0\ \text{ as }\ y \to \infty \end{cases} \end{aligned} \tag{18}$$

where, $G_r = \frac{\upsilon g\beta}{U_0^3}(T_w - T_\infty)$ = Grashof number; $G_m = \frac{\upsilon g\beta^*}{U_0^3}(C_w - C_\infty)$ = Solutal Grashof number; $H_a = \frac{\upsilon\sigma B_0^2}{\rho U_0^2}$ = Hartmann number; $P_r = \frac{\rho c_p \upsilon}{k}$ = Prandtl number; $D_f = \frac{D_m k_T}{\upsilon c_s c_p}\frac{(C_w - C_\infty)}{(T_w - T_\infty)}$ = Dufour number; $S_c = \frac{\upsilon}{D_m}$ = Schmidt number.

3 Method of solutions

The dimensionless, nonlinear, coupled partial differential Eqs. (13)–(17) together with associated boundary conditions (18) are solved by using the explicit finite difference

method. The maximum length of the plate is taken $x_{\max}(= 40)$ and the maximum length of the boundary layer is $y_{\max}(= 25)$ corresponding to $y \to \infty$. This means x varies from 0 to 40 and y varies from 0 to 25. The finite difference schemes for some variables with respect to t, x and y as follows:

$$\frac{\partial u}{\partial t} = \frac{U_{i,j}^{k+1} - U_{i,j}^{k}}{\Delta t}; \quad \frac{\partial u}{\partial x} = \frac{U_{i,j}^{k} - U_{i-1,j}^{k}}{\Delta x}; \quad \frac{\partial u}{\partial y} = \frac{U_{i,j}^{k} - U_{i,j-1}^{k}}{\Delta y}; \quad \frac{\partial^2 u}{\partial y^2} = \frac{U_{i,j+1}^{k} - 2U_{i,j}^{k} + U_{i,j-1}^{k}}{(\Delta y)^2}.$$

Here the subscript 'i' refers to x; 'j' to y and superscript 'k' refers to time t. Similarly, we have used finite difference schemes for the other variables. We have used Matlab code to get the solution of finite difference schemes and its graphical presentation.

3.1 Shear stresses, Nusselt number and Sherwood number

The effects of various parameters on local and average shear stress have been investigated from the velocity profile. The velocity gradient at the plate is defined as the shear stress; the non-dimensional form of the local shear stress and average shear stress in x-direction are given by the relations $\tau_L = \mu \frac{\partial u}{\partial y}\Big|_{y=0}$ and $\tau_A = \frac{1}{L}\int_0^L \mu \frac{\partial u}{\partial y}\Big|_{y=0} dx$ respectively. From the temperature profile, the effects of various parameters on local and average Nusselt number have been calculated. The rate of heat transfer at the plate is defined as the Nusselt number; the local Nusselt number and the average Nusselt number are given by $Nu_L = -\mu \frac{\partial \theta}{\partial y}\Big|_{y=0}$ and $Nu_A = -\frac{1}{L}\int_0^L \mu \frac{\partial \theta}{\partial y}\Big|_{y=0} dx$ respectively. Similarly, we have analyzed the effects of various parameters on local and average Sherwood number from the concentration field. The rate of mass transfer at the plate is defined as the Sherwood number; the local Sherwood number and the average Sherwood number are defined by $Sh_L = -\mu \frac{\partial \varphi}{\partial y}\Big|_{y=0}$ and $Sh_A = -\frac{1}{L}\int_0^L \mu \frac{\partial \varphi}{\partial y}\Big|_{y=0} dx$ respectively.

4 Results and discussion

To observe the physical situiation of the problem, the effects of pertinent parameters on flow patterns of the velocity, heat, and mass transfer processes have been investigated. The validation of the results is shown in the following paragraph by comparing the current results with previously published results on the common effects on the primary velocity, secondary velocity, temperature concentration, Nusselt number, and Sherwood number.

4.1 Comparison and validation

Figure 2a, b and the Table 1 present a comparison our numerical results with recently

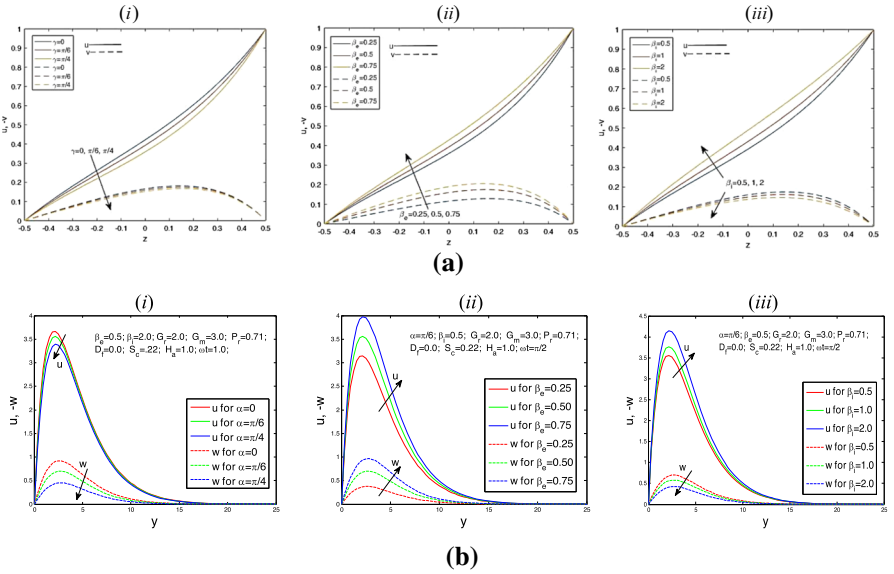

Fig. 2 **a** [Singh and Vishwanath (2020) experiment]. Velocity distribution for different values of (*i*) inclined angle γ (*ii*) Hall parameter β_e (*iii*) Ion-slip parameter β_i. **b** [Current experiment] Velocity distribution for different values of (*i*) inclined angle α (*ii*) Hall parameter β_e (*iii*) Ion-slip parameter β_i

Table 1 Comparison our numerical results with recently published experiments

Effects of	On	Our Current Result	Results of Singh and Vishwanath (2020)	Results of Krishna et al. (2020)
Inclined angle	primary velocity	Dec.	Dec.	
	secondary velocity	Inc.	Inc.	
Hall Parameter	primary velocity	Inc.	Inc.	
	secondary velocity	Dec.	Dec.	
Ion-slip Parameter	primary velocity	Inc.	Inc.	
	secondary velocity	Inc.	Inc.	
Prandtl number	temperature	Dec.		Dec.
	Nusselt number	Inc.		Inc.
Schmidt number	concentration	Dec.		Dec.
	Sherwood number	Inc.		Inc.

published experiments. The results of the present research in fluid flow have been compared with the experiment of Singh and Vishwanath [28] and Krishna et al. [29]. Some of common effects of the parameters on the fluid flow are displayed by graphical and tabular form as follows:

Figure 2a exhibits Singh and Vishwanath (2020) experiment of the velocity distribution u and w for different values of (i) inclined angle γ (ii) Hall parameter β_e (iii) Ion-slip parameter β_i and Fig. 2b exhibits our present experiment of the velocity distribution u and w for different values of (i) inclined angle α (ii) Hall parameter β_e (iii) Ion-slip parameter β_i with fixed values of the parameters $\alpha = \pi/6$, $\beta_e = 0.5$, $\beta_i = 0.5$, $G_r = 2.0$, $G_m = 3.0$, $H_a = 1.0$, $P_r = 0.71$, $D_f = 0.0$, $S_c = 0.22$ and $\omega t = \pi/2$. Same behaviors of the flow patterns are found for the corresponding graphs of both experiments. Also Table 1 displays a comparison of our results with the experiments of Singh and Vishwanath [28] and Krishna et al. [29] in literature form. From the above comparison, it can be concluded that the current result should be valid with the existing results.

The current results carried for the influence of the relevant non-dimensional parameters namely Hartmann number (H_a), thermal Grashof number (G_r), solutal Grashof number(G_m), Hall parameter (β_e), Ion-slip parameter (β_i), Prandtl number (P_r), Dufour number (D_f) and Schmidt number (S_c) on various distributions such as on the velocity, temperature, concentration, local and average shear stress, local and average Nusselt number, local and average Sherwood number. The effects of those parameters on some important profiles are shown in Figs. 5, 6, 7, 8, 9, 10, 11, 12, 13, 14, 15, 16, 17, 18, 19, 20, 21, 22, 23, 24, 25, 26, 27, 28, 29, 30, 31, 32, 33, 34, 35 and 36.

4.2 Time and mesh sensitivity test

For the time sensitivity, the computations have been carried out for different maximum time $t = 3, 7, 11, 15, 18$ and 20 with time increment $\Delta t = 0.01$ on the velocity profile which is shown in Fig. 3a. It has been seen from the figure that the velocities are very minimal change after $t = 15$, therefore the steady-state solutions are considered

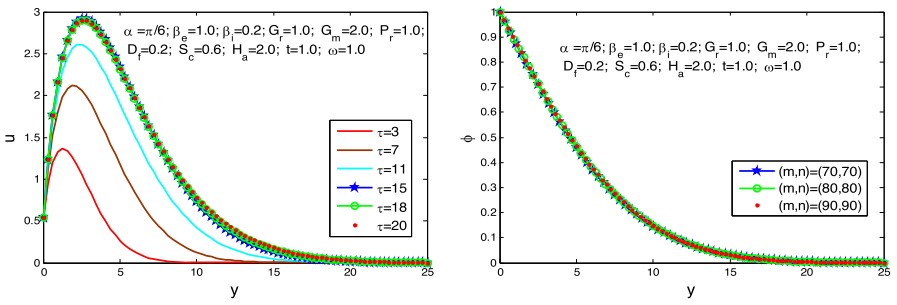

Fig. 3 **a** Time sensitivity on u for different values of maximum time 'τ'. **b** Mesh sensitivity on φ for different values of mesh spaces (m, n)

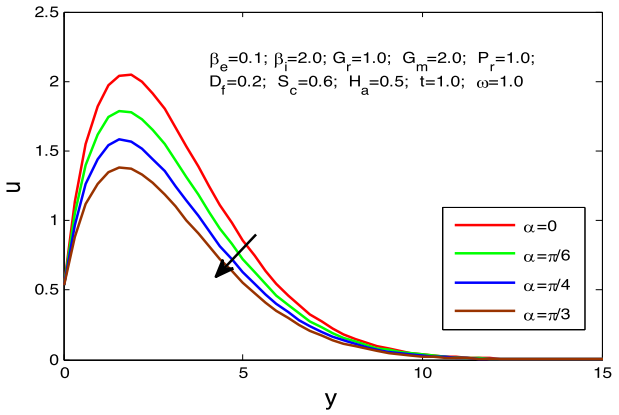

Fig. 4 Primary velocity distribution u for different values of inclined angle α

for the time $t = 15$ with time increment $\Delta t = 0.01$. Also for mesh sensitivity, the computations have been carried out for different mesh spaces such as $(m\,,\,n) = (70, 70)$; $(m\,,\,n) = (80\,,\,80)$ and $(m\,,\,n) = (90, 90)$ within the intervals $0 \leq x \leq 40$ & $0 \leq y \leq 25$ on the concentration, which is shown in Fig. 3b. It is observed from the figure that there is a negligible change with different meshes. From those pairs of mesh points, we have chosen $(m\,,\,n) = (80\,,\,80)$ for our computations. The same situation for the other distributions for steady-state time and mesh.

4.3 Primary velocity distributions

At first, it is mentioned from our physical configuration of the model that "the plate is inclined means induced magnetic field is also inclined because the induced magnetic field is applied to the right angle to the plate". Figure 4 indicates that the primary velocity u decreases with the increase of inclined angle α. It is observed that the velocity in x-direction is highly increasing when the plate is properly vertical, i.e. when $\alpha = 0$. Figures 5, 6, 7, 8 and 9 elucidate the influence of pertinent parameters on the primary velocity u for different values of β_e, G_r, H_a, P_r and D_f with the fixed value of $\alpha = \pi/6$(or,$\alpha = \pi/3$).

Figure 5 shows that the velocity u increases with the increase of β_e. But from Fig. 6 it is found in the main portion of the boundary layer that the velocity u increases with the increase of Grashof number G_r. But the velocity is decreased with the increasing value of H_a and P_r, which have shown in Figs. 7 and 8. It is observed from Fig. 9 that u has a minor increasing effect with the increase of D_f.

4.4 Secondary velocity distributions

Figure 10 exhibits the secondary velocity w increases with the increase of inclined angle α, but it has a negative flow. Figures 11, 12, 13, 14 and 15 indicate that the effect of parameters β_e, β_i, P_r and D_f on the secondary velocity w with the fixed

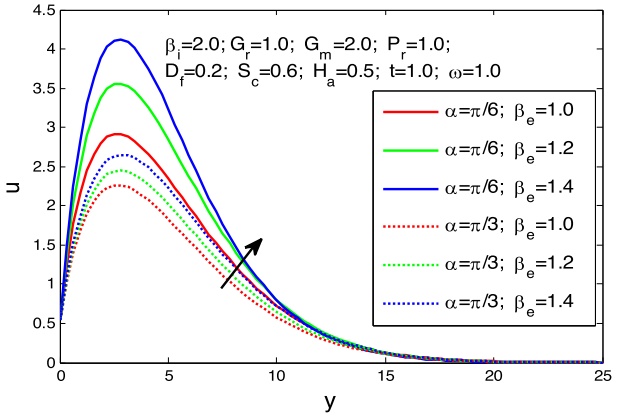

Fig. 5 Primary velocity distribution u for different values of Hall parameter β_e

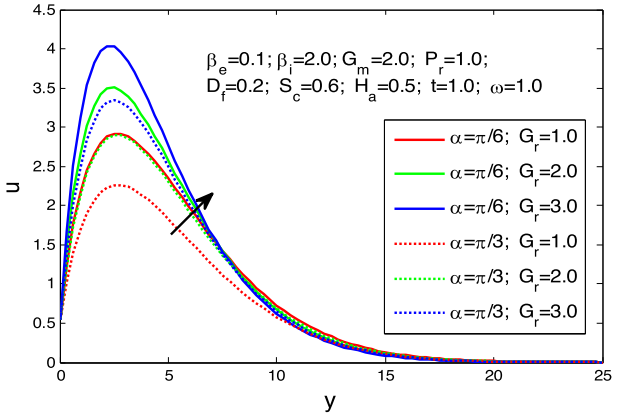

Fig. 6 Primary velocity distribution u for different values of Grashof number G_r

value of $\alpha = \pi/6$ (or, $\pi/3$). It is observed that the velocities are much affected by the inclined angle α. Figure 11 indicates that w decreases with the increase of β_e. But from Figs. 12, 13 and 14 notice that the velocity w increases with the increase of β_i, H_a, P_r. The secondary velocity is decreased with the increasing value of D_f, which have been shown in Fig. 15.

4.5 Temperature distributions

Figure 16 depicts the influence of the effective inclined angle α on the fluid temperature θ. It is seen from the figure that the temperature is increased with the increase of α. From Figs. 17, 18 and 19, it has been investigated that the temperature is decreased with the increase of β_e, G_r and P_r, whereas the temperature is increased with the increase of D_f and S_c, which is shown in Figs. 20, and 21.

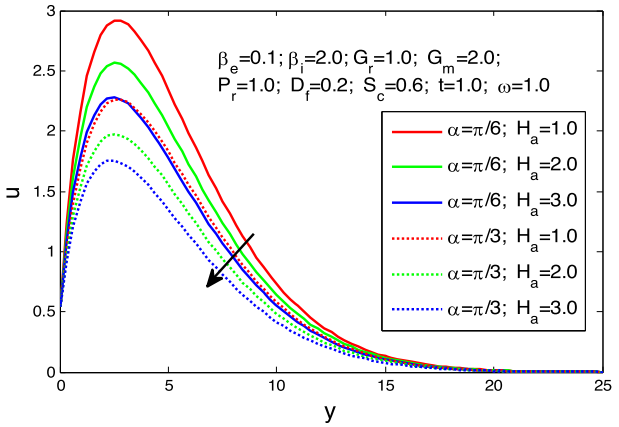

Fig. 7 Primary velocity distribution u for different values of Hartmann number H_a

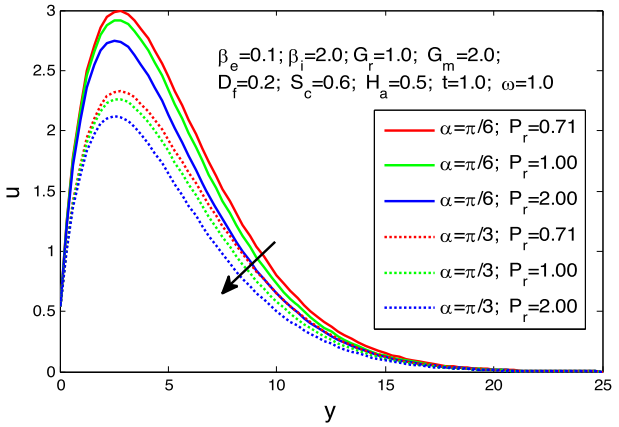

Fig. 8 Primary velocity distribution u for different values of Prandtl number P_r

4.6 Concentration distributions

Figure 22 represents the effect of inclined angle α on the fluid concentration φ. It has been indicated that the concentration is increased with the increase of α. From Figs. 23, 24 and 25, it is analyzed for all cases that the concentration is decreased with the increase of β_e, G_m and S_c.

4.7 Local and average shear stress

Noted that the figures (a) and (b) of Figs. 26, 27, 28, 29, 30, 31, 32 and 33 are represented the local shear stress (τ_L) and average shear stress (τ_A) respectively. Figure 26 depicts the effect of inclined angle α on the primary shear stress. It has been seen that in both

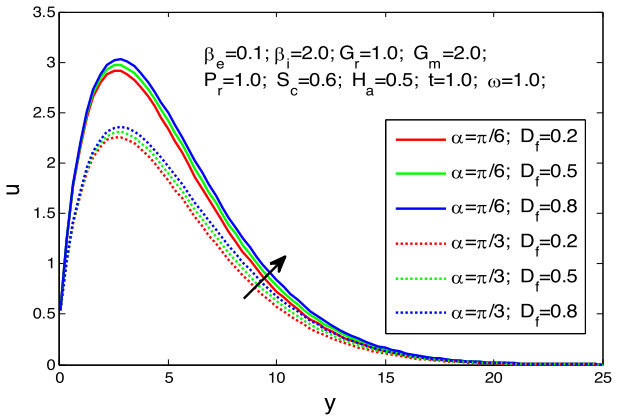

Fig. 9 Primary velocity distribution u for different values of Dufour number D_f

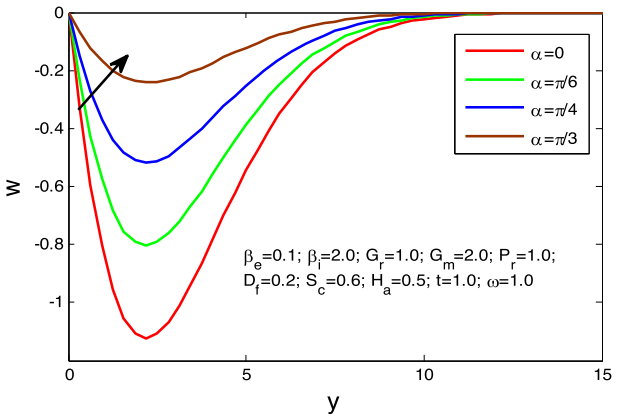

Fig. 10 Secondary velocity distribution w for different values of inclined angle α

cases, the primary velocity gradient along x-direction of the plate decreases with the increase of α. From Figs. 27, 28, it is analyzed that the primary shear stress increases with the increase of β_e and G_r. But from Fig. 29, it has been seen that primary shear stress decreases with the increase of H_a.

On the other hand, Fig. 30 describes the effect of inclined angle α on the secondary shear stress. Here in both cases, the secondary velocity gradient along x-direction at the plate is increased with the increase of α. Figure 31 shows that the secondary shear stress is increased with the increase of β_i. But Figs. 32, 33 show the decreasing effect with the increase of β_e and D_f. It is observed that the effects of susceptive parameters on local shear stress, average shear stress and on velocity distributions have same.

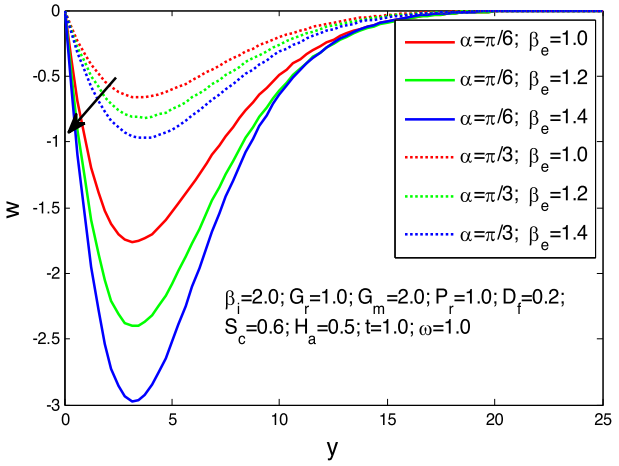

Fig. 11 Secondary velocity distribution w for different values of Hall parameter β_e

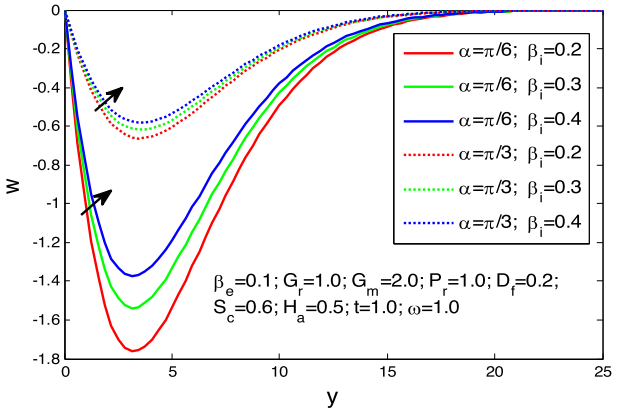

Fig. 12 Secondary velocity distribution w for different values of Ion-slip parameter β_i

4.8 Local and average Nusselt number, Sherwood number

The figures (a) and (b) of Figs. 34, and 35 are represented the local Nusselt number (Nu_L) and average Nusselt number (Nu_A). And figures (a) and (b) of Fig. 36 are represented the local Sherwood number (Sh_L) and average Sherwood number (Sh_A) respectively. Figure 34 exhibits the effect of D_f on the Nusselt number. It has seen that the concentration gradient at the wall decreases with the increase of D_f.But Fig. 35 shows that the Nusselt number is increased with the increase of P_r. On the other hand, the Sherwood number increases with the increase of S_c, which is shown in Fig. 36.

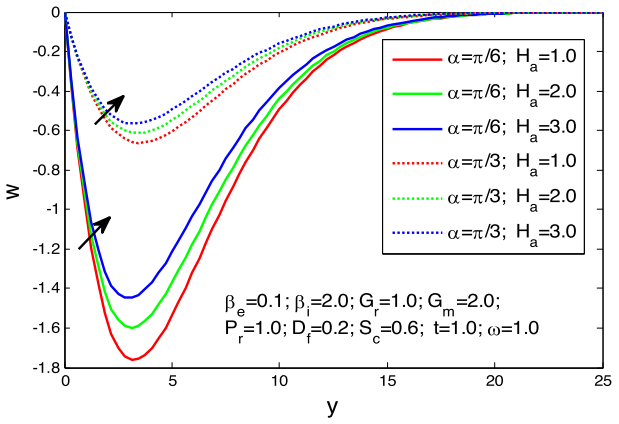

Fig. 13 Secondary velocity distribution 'w'for different values of Hartmann number 'H_a'

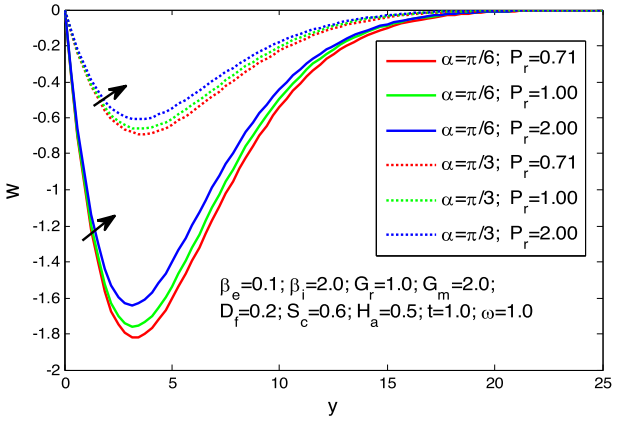

Fig. 14 Secondary velocity distribution w for different values of Prandtl number P_r

5 Conclusions

The influence of Hall and Ion-slip currents on unsteady MHD fluid flow with Dufour effects over an inclined plate and inclined magnetic field is explored in this study. The presence of Hall and Ion-slip currents effects offers to capitulate to the increase of velocity distribution thereby acting like an overprotective device for preventing front flow, whereas the angle of inclination, Hartmann number, and the Prandtl number reduces the flow in the direction perpendicular to the main flow. Particular findings of our study are summarized as follows.

- Primary velocity u rises with the increase of β_e, G_r and D_f while it decreases with the increase of α,H_a and P_r.
- Secondary velocity w increases with the increase of α, β_i, H_a and P_r, it has a decreasing effect with the increase of β_e and D_f.

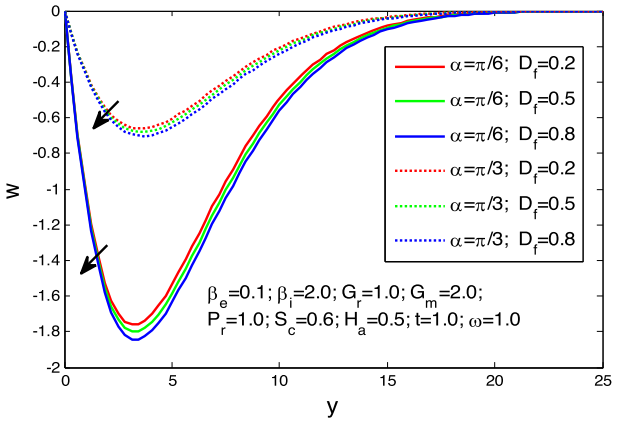

Fig. 15 Secondary velocity distribution w for different values of Dufour number D_f

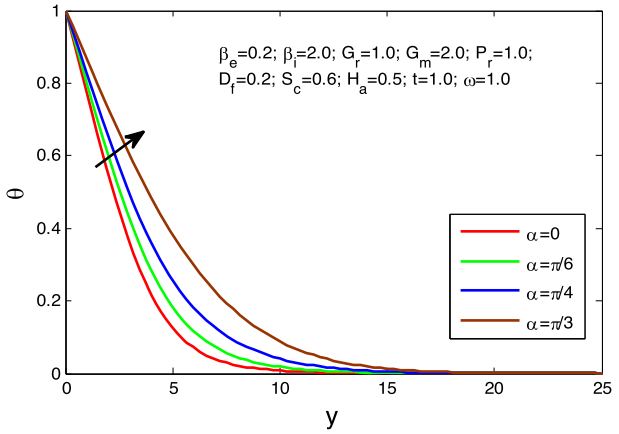

Fig. 16 Temperature distribution θ for different values of inclined angle α

- Temperature θ is improved with the increase of α, S_c and S_c, whereas it has a decreasing effect with the increase of β_e, G_r and P_r.
- Concentration φ is increased with the increase of α, whereas it has been decreasing effect with the increase of β_e, G_m and S_c.

Since most of the universe is filled with vastly charged particles and surrounded by a magnetic field, the application of Hall and Ion-slip current on the flow plays a significant role to improve the performance of the mechanical device, and it helps to perform reliable analysis mathematically for fluid flow.

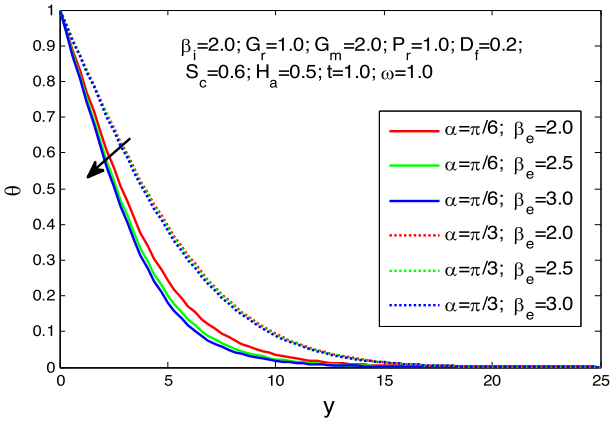

Fig. 17 Temperature distribution θ for different values of Hall parameter β_e

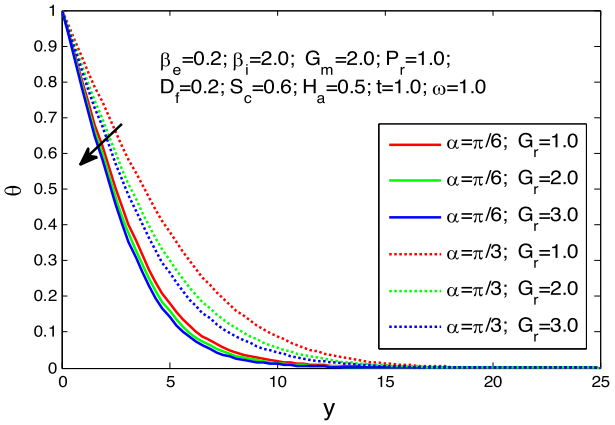

Fig. 18 Temperature distribution θ for different values of thermal Grashof number G_r

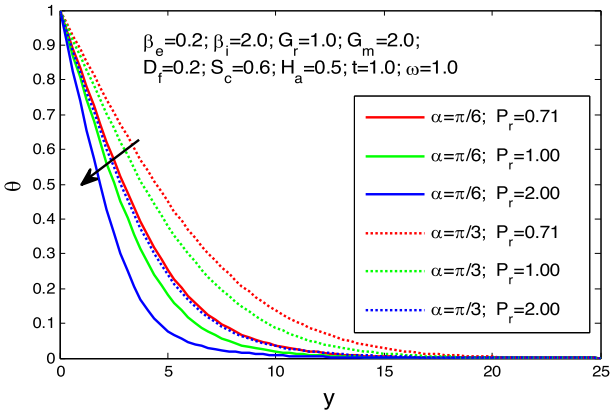

Fig. 19 Temperature distribution θ for different values of Prandtl number P_r

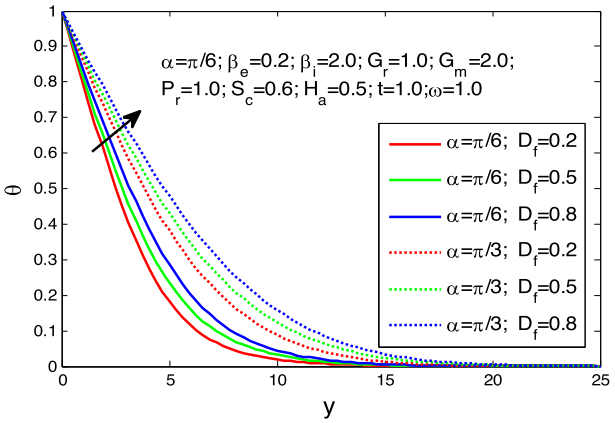

Fig. 20 Temperature distribution θ for different values of Dufour number D_f

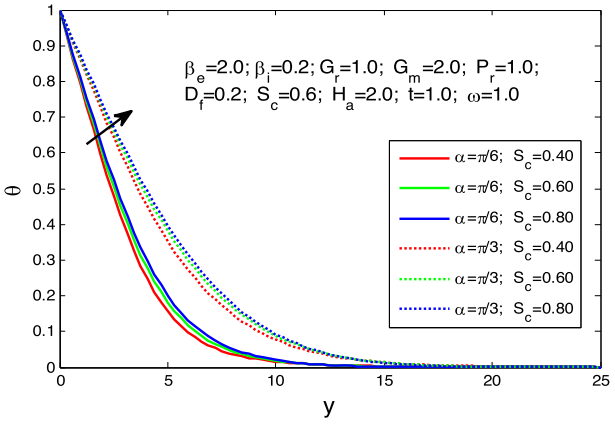

Fig. 21 Temperature distribution θ for different values of Schmidt number S_c

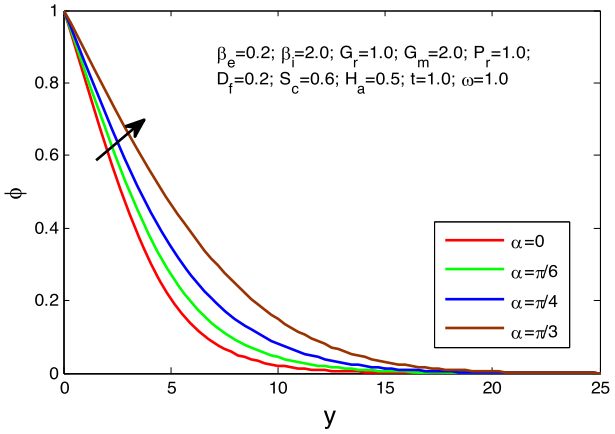

Fig. 22 Concentration distribution φ for different values of inclined angle α

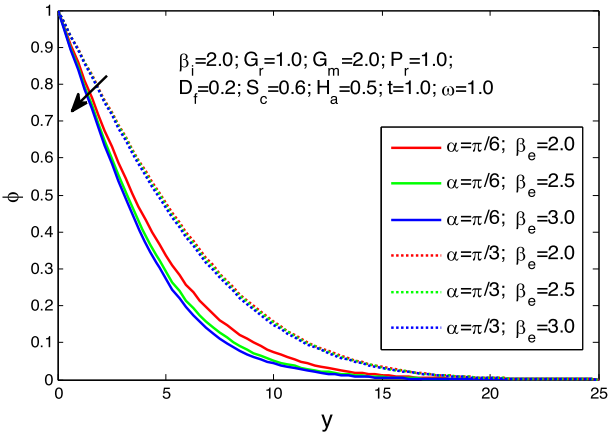

Fig. 23 Concentration distribution φ for different values of Hall parameter β_e

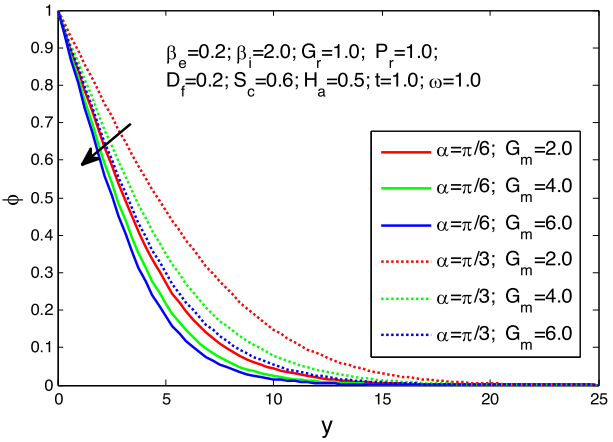

Fig. 24 Concentration distribution φ for different values of mass Grashof number G_m

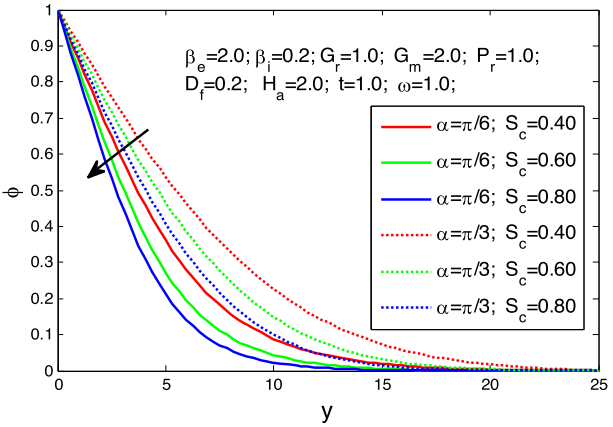

Fig. 25 Concentration distribution φ for different values of Schmidt number S_c

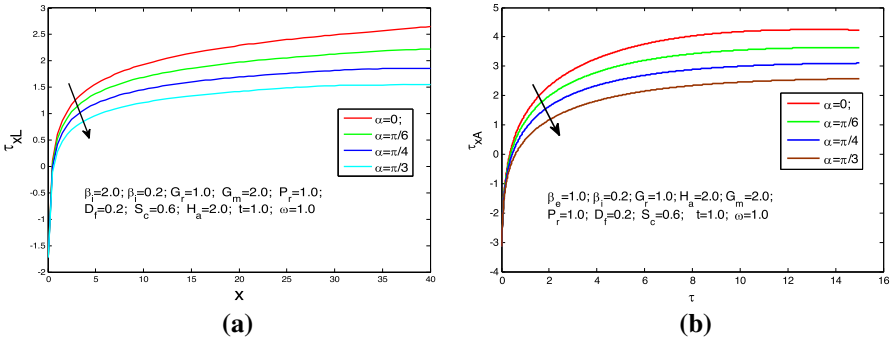

Fig. 26 a Local primary Shear stress τ_{xL} for different values of inclined angle α. **b** Average primary Shear stress τ_{xA} for different values of inclined angle α

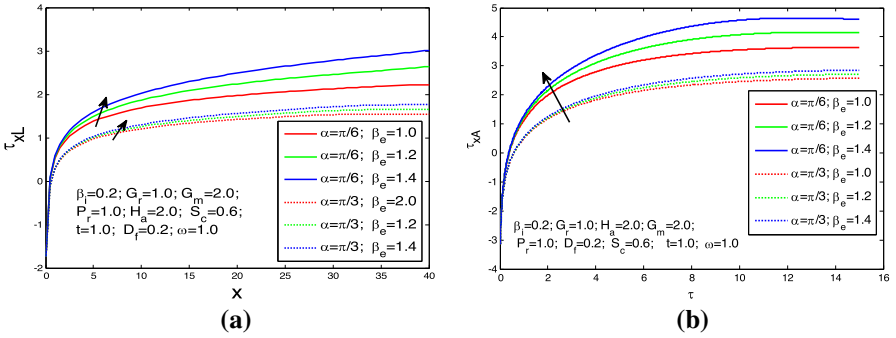

Fig. 27 a Local primary Shear stress τ_{xL} for different values of Hall parameter β_e. **b** Average primary Shear stress τ_{xA} for different values of Hall parameter β_e

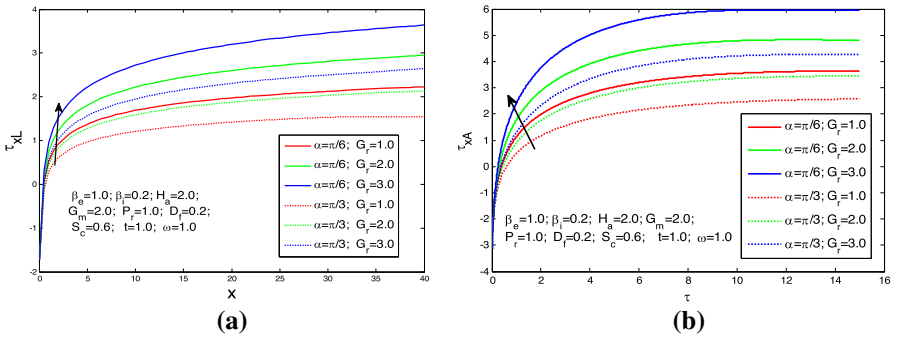

Fig. 28 a Local primary Shear stress τ_{xL} for different values of thermal Grashof number G_r. **b** Average primary Shear stress τ_{xA} for different values thermal Grashof number G_r

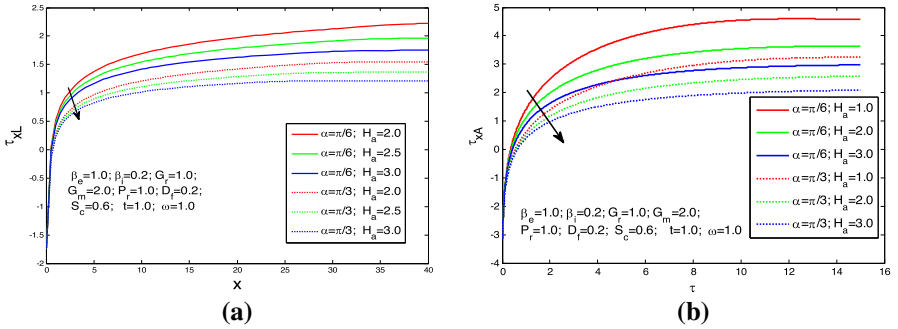

Fig. 29 a Local primary Shear stress τ_{xL} for different values of Hartmann number H_a. **b** Local primary Shear stress τ_{xL} for different values of Hartmann number H_a

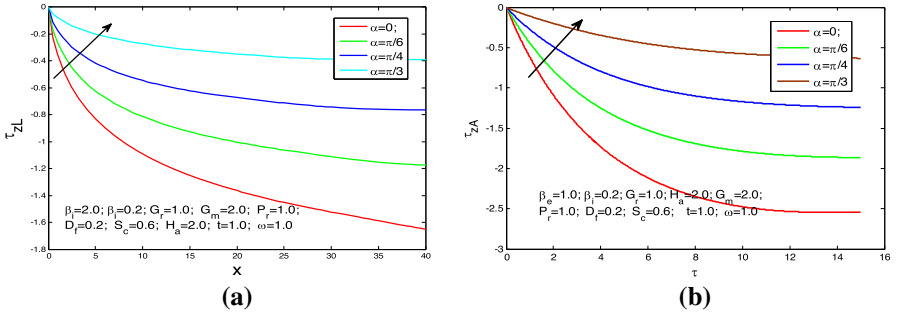

Fig. 30 a Local secondary Shear stress τ_{zL} for different values of inclined angle α. **b** Average secondary Shear stress τ_{zA} For different values of inclined angle α

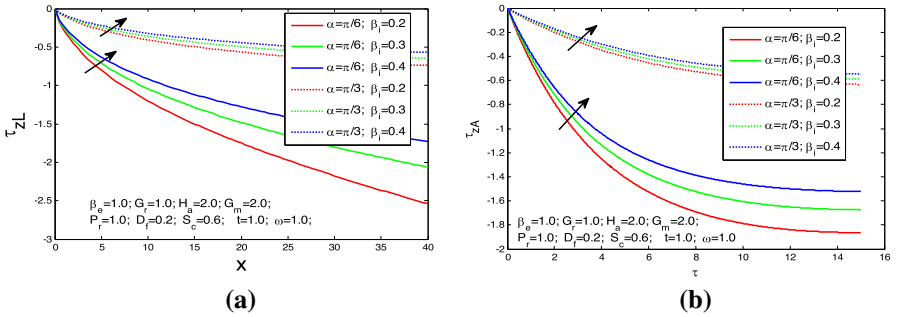

Fig. 31 **a** Local secondary Shear stress τ_{zL} for different values of Ion-slip parameter β_i. **b** Average secondary Shear stress τ_{zA} for different values of ion-slip parameter β_i

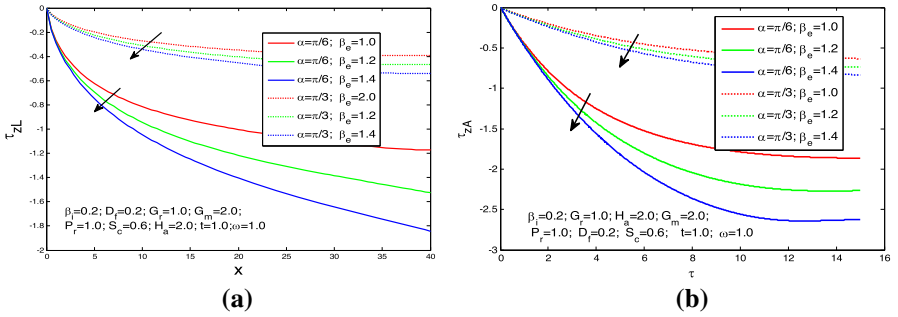

Fig. 32 **a** Local secondary Shear stress τ_{zL} for different values of Hall parameter β_e. **b** Average secondary Shear stress τ_{zA} for different values of Hall parameter β_e

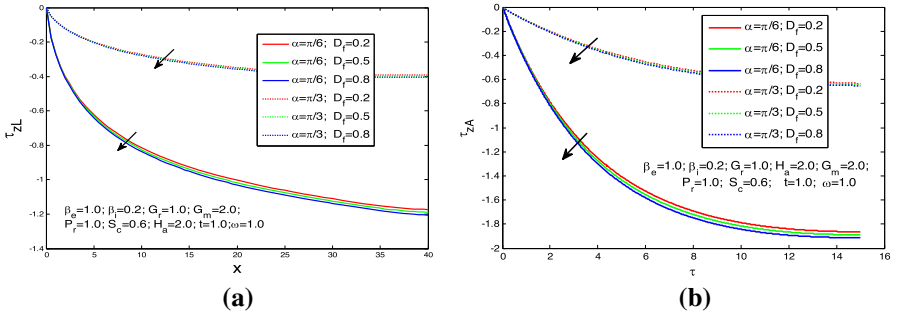

Fig. 33 **a** Local secondary Shear stress τ_{zL} for different values of Dufour number D_f. **b** Average secondary Shear stress τ_{zA} for different values of Dufour number D_f

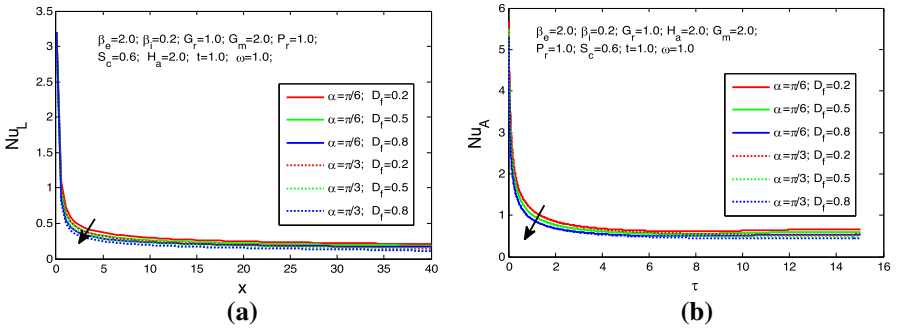

Fig. 34 **a** Local Nusselt number Nu_L for different values of Dufour number D_f. **b** Average Nusselt number Nu_A for different values of Dufour number D_f

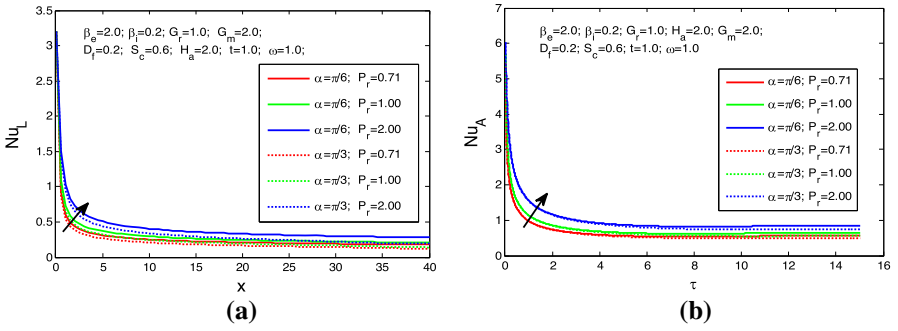

Fig. 35 **a** Local Nusselt number Nu_L for different values of Prandtl number P_r. **b** Average Nusselt number Nu_A for different values of Prandtl number P_r

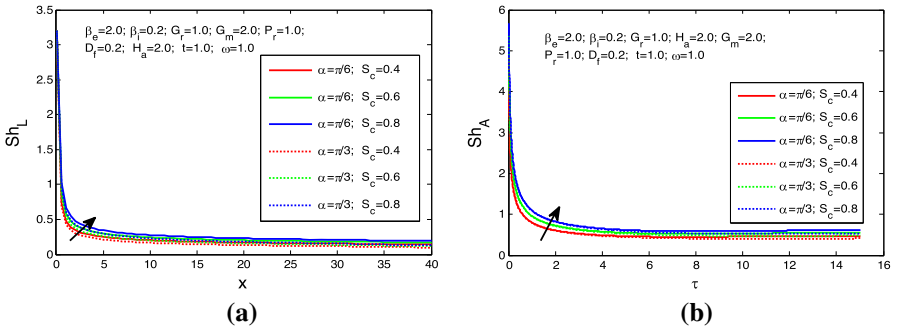

Fig. 36 a Local Sherwood number Sh_L for different values of Schmidt number S_c. **b** Average Sherwood number Sh_A for different values of Schmidt number S_c

Author Contributions M. R. Islam and M. M. Alam have written the literature review. M. R. Islam and S. Nasrin have developed the geometrical configuration, and illustrated the algorithm and written codes by using MATLAB R2015a tools. M. R. Islam and S. Nasrin has drawn the graphs and written the manuscript. All authors have checked the code and the simulated data.

Declarations

Conflict of interest It is declaring that, on behalf of all authors, the corresponding author states that there is no conflict of interest; we have no affiliations or involvement with an organization with a financial or non-financial interest in this research.

References

1. Abel, S., Veena, P.H.: Visco-elastic fluid flow and heat transfer in porous medium over a stretching sheet. Int. J. Non-Linear Mech. **33**, 531–540 (1998)
2. Abernathy, F.H.: Flow over an inclined plate. J. Fluids Eng. **84**(3), 380–388 (1962)
3. Ajay, K.S.: MHD free convection and mass transfer flow with Hall current, viscous dissipation, joule heating and thermal diffusion. Indian J. Pure Appl. Phys. **41**, 24–35 (2003)
4. Angirasa, D., Peterson, G.P.: Natural convection heat transform from an isothermal vertical surface to a fluid saturated thermally stratified porous medium. Int. J. Heat Mass Transfer **14**(8), 4329–4335 (1997)
5. Basant, K.J., Peter, B.M.: Hall current and ion-slip effects on free convection flow in a vertical micro channel with an induced magnetic field". Heat Transf. Asian Res. (2019). https://doi.org/10.1002/htj.21569
6. Beg, O.A., Sim, J.L., Zueco, R., Bhargava, R.: Numerical study of magneto-hydrodynamic viscous plasma flow in rotating porous media with Hall currents and inclined magnetic field influence. Commun. Nonlinear Sci. Numer. Simul. **15**, 345–359 (2010)
7. Bhpendra, K.S., Abhay, K.J., Chaudhary, R.C.: Hall effect on MHD mixed convective flow of a viscous incompressible fluid past a vertical porous plate immersed in porous medium with heat source/sink. Rom. J. Phys. **52**, 5–7 (2007)
8. Daniel, S., Daniel, Y.S.: Convective flow two immiscible fluids and heat transfer with porous along an inclined channel with pressure gradient. Int. J. Eng. Sci. **2**(4), 12–18 (2013)
9. Eraslan, A.H.: Temperature distributions in MHD channels with Hall effect. AIAAJ **7**, 186–188 (1969)
10. Gupta, P.S., Gupta, A.S.: Heat and mass transfer on a stretching sheet with suction or blowing. Can. J. Chem. Eng. **55**, 744–746 (1997)
11. Javeri, V.: Combined influence of Hall effect, ion slip, viscous dissipation and Joule heating on MHD heat transfer in a channel. Heat Mass Transf. **8**, 193–202 (1975)

12. Jyotsna, R.P., Gouranga, C.D., Suprava, S.: Radiation and mass transfer effects on MHD flow through porous medium past an exponentially accelerated inclined plate with variable temperature. Ain Shams Eng. J. **8**, 67–75 (2017)
13. Kumar, B.V.R., Singh, P.: Effect of thermal stratification on free convection in a fluid saturated porous enclosure. Numer. Heat Transf. **34**, 343–356 (1999)
14. Singh, N.K., Kumar, V., Sharma, G.K.: The effect of inclined magnetic field on unsteady flow past on moving vertical plate with variable temperature. IJLTEMAS **5**(2), 34–37 (2016)
15. Opanuga, A.A., Agboola, O.O., Okagbue, H.I., Olanrewaju, A.M.: Hall current and ion-slip effects on the entropy generation of couple stress fluid with velocity slip and temperature jump. Int. J. Mech. **12**, 221–231 (2018)
16. Prasada, V., Sivaprasad, R., Rao, U.R.: Hall effects on hydromagnetic channel flow under an inclind magnetic field. Indian Natn. Sci. Acad. **52**(3), 573–583 (1986)
17. Rajput, U.S., Gupt, N.K.: Dafour effect on unsteady free convection MHD flow past an exponentially accelerated plate through porous media with variable temperature and constant mass diffusion in an inclined magnetic field. IRJET **3**(8), 2135–2140 (2016)
18. Ram, P.C.: The effect of Hall and ion slip current on free convection heat generating flow in a rotating fluid. Int. J. Energy Res. **19**(5), 371–376 (1995)
19. Hanvey, R.R., Khare, R.K., Paul, A.: MHD flow of incompressible fluid through parallel plates in inclind magnetic field having porous medium with heat and mass transfer. IJSIMR **5**(4), 18–22 (2017)
20. Sato, H.: The Hall effect in the viscous flow of ionized gas between two parallel plates under transverse magnetic field. J. Phys. Soc. Jpn. **16**, 1427–1433 (1961)
21. Seth, G.S., Nandkeolyar, R., Mahto, N., Singh, S.K.: MHD couette flow in a rotating system in the presence of an inclined magnetic field. Appl. Math. Sci. **3**(59), 2919–2932 (2009)
22. Seth, G.S., Nandkeolyer, R., Ansary, M.S.: Hartmann flow in a rotating system in the present of inclined magnetic field with Hall effects. Tamkang J. Sci. Eng. **13**(3), 243–252 (2010)
23. Seth, G.S., Mandal, P.K., Chamkha, A.J.: MHD free convection flow past an impulsively moving vertical plate with ramped heat flux through porous medium in the presence of inclined magnetic field. FHMT **7**, 23 (2016)
24. Agarwalla, S., Ahmed, N.: MHD mass transfer flow past an inclined plate with variable temperature and plate velocity embedded in a porous medium. Heat Transf. **47**(1), 27–41 (2018)
25. Singh, J.K., Joshi, N., Begum, S.G., Srinivasa, C.T.: Unsteady hydromagnetic heat and mass transfer natural convection flow past an exponentially accelerated vertical plate with Hall current and rotation in the presence of thermal and mass diffusions. Front. Heat Mass Transf. (FHMT) **7**, 24 (2016). https://doi.org/10.5098/hmt.7.24
26. Singh, J.K., Joshi, N., Rohidas, P.: Unsteady MHD natural convective flow of a rotating walters'-b fluid over an oscillating plate with fluctuating wall temperature and concentration. J. Mech. **34**(4), 519–532 (2018). https://doi.org/10.1017/jmech.2017.25
27. Singh, J.K., Seth, G.S., Joshi, N., Srinivasa, C.T.: Mixed convection flow of a viscoelastic fluid through a vertical porous channel influenced by a moving magnetic field with Hall and ion-slip currents, rotation, heat radiation and chemical reaction. Bulg. Chem. Commun. **52**(1), 147–158 (2020). https://doi.org/10.34049/bcc.52.1.468
28. Singh, J.K., Vishwanath, S.: Hall and ion-slip effects on MHD free convective flow of a viscoelastic fluid through porous regime in an inclined channel with moving magnetic field. Kragujevac J. Sci. **42**, 5–18 (2020)
29. Krishna, M.V., Ahmad, N.A., Chamkha, A.J.: Hall and ion slip effects on unsteady MHD free convective rotating flow through a saturated porous medium over an exponential accelerated plate. Alex. Eng. J. **59**(2), 565–577 (2020)